Supporting Information for

Reconstructing the Tectonic History of the Arabian–Nubian Shield in Sinai: Low-Temperature Thermochronology Implications on Wadi Agar Area

Sherif Mansour [1,*], Noriko Hasebe [2], Kamal Abdelrahman [3], Mohammed S. Fnais [3] and Akihiro Tamura [4]

[1] Geology Department, Faculty of Science, Port Said University, Port Said 42522, Egypt
[2] Institute of Nature and Environmental Technology, Kanazawa University, Kanazawa 920-1192, Japan
[3] Department of Geology & Geophysics, College of Science, King Saud University, P.O. Box 2455, Riyadh 11451, Saudi Arabia
[4] Department of Earth Sciences, Kanazawa University, Kanazawa 920-1192, Japan
* Correspondence: sherif@sci.psu.edu.eg; Tel.: +20-10-9001-2146

Introduction

This file provides more details on the sedimentological cover of the Gulf of Suez region, which shows how the depositional environments were changed through time. These data were integrated with our findings to provide robust tectonic interpretations for the obtained results. Furthermore, we provide here more details on used thermochronology techniques and the analytical methods. Supporting figures from our research and detailed data tables are also provided.

Text S2. Sedimentologic Cover

The lithostratigraphic sequence in the Gulf of Suez region stretches from the Cambrian to Recent (Fig. 3), and can be classified into: A) The Paleozoic succession (Fig. 3), which was originally divided into three mappable units (Barron, 1907; Hassan, 1967; Said, 1971); A1) The Qebliat Group (Cambrian age, ~130 m thick), formed from cycles of fluvial to near-shore marine sediments (Hassan, 1967; Said, 971; Bosworth et al., 2005). A2) The Um Bogma Formation (Carboniferous age, ~225 m thick), comprises dolomite, sandy marl, and intercalations of silt and sandstone (Kora, 1984; McClay et al., 1998). A3) The Abu Thora Formation (Carboniferous age, ~214 m thick), comprises varicolored interbedded fluvial sandstone with nearshore marine sandstone, siltstone, shale, and locally thin coal seams. The upper part of the Abu Thora Formation contains basalt sills at several localities (Kostandi, 1959; Weissbrod, 1969; Kora, 1984). By the end of the Carboniferous, the Gulf of Suez region was uplifted as indicated by the lack of any Permian marine sediments (Klitzsch and Wycisk 1978; Klitzsch 1990).

B) The Mesozoic succession in the Gulf of Suez region spans the Triassic to the Late Cretaceous (Fig. 3); B1) The Qiseib Formation (Triassic age, ~327 m thick), consists of a lower variegated shale, siltstones, sandstones, and an upper thin clastic carbonate unit (Weissbrod, 1969; Abdallah and Adindani, 1963). B2) The Malha Formation (Lower Cretaceous age, ~149 m thick), comprises a lower Member of shale, clay, sandstone with conglomerate, and an upper Member of tabular and cross-bedded sandstone (Sultan, 1985; Abu-Zied, 2007; Kassem et al., 2021). B3) The Raha to Sudr Formations (Upper Cretaceous age), representing a shallow marginal marine environment characterized by a mix of clastic and carbonate sequences (e.g., Osman,1954; El Sharawy and Nabawy, 2016; Shehata et al., 2021).

C) The Cenozoic sequence spans the Palaeocene to Quaternary (Fig. 3), and consists of; C1) The Esna Formation (Palaeocene age, ~35 m thick), consists of dark greenish shale unit and 1 m carbonate thin beds (Said, 1990a). C2) The Thebes and Mokattam Formations (Lower Eocene and Middle-Upper Eocene age, respectively), are represented mostly by chalky limestones with thin-bedded flint bands (Said, 1960; McClay et al., 1998; El-Azabi, 2006). C3) The Tayiba Formation (Oligocene age, ~152 m thick), which unconformably

overlies the Mokattam Formation (Ibrahim et al., 2016), and marks the transition from the pre-rifting Eocene marine sediments to the Early Miocene rift forming transgression sediments (Refaat and Imam 1999). C4) The Nukhul (Abu Zenima) Formation (Lower Miocene age, ~100 m thick), which unconformably overlies Tayiba Formation, and contains alluvial and volcanic deposits from the early syn-rift stage (El- Moustafa and Yousif, 1993; Abou El-Anwar, 2019). C5) The Rudeis Formation (Lower-Middle Miocene age, ~191 m thick), conformably overlies the Nukhul Formation and is characterized by deep marine sediments (El Heiny and Martini, 1981; Sallam et al., 2019). C6) The Kareem, Belayim, South Gharib, and Zeit Formations (Middle-Late Miocene age, ~1250 m thick), which conformably overly the Rudeis Formation and each other. They are dominated by evaporites and intercalations of sandstones and shales (El Naggar, 1988; Tewfik et al., 1992; Darwish and ElAraby, 1994; Sallam et al., 2019). C7) The Zafarana Wardan Formation (Pliocene age, ~120 m thick), is represented by sandstone and clay streaks (El Naggar, 1988; Tewfik et al., 1992; Sallam et al., 2019).

Text S3. Methods

S3.1 Fission-Track Thermochronology

The ZFT and AFT were analyzed at the Kanazawa Uni. thermochronology lab., where Laser Ablation Inductively Coupled Plasma Mass Spectrometry (LA-ICP-MS) was applied for direct measurement of the U concentrations (Hasebe et al., 2004). The detailed operating conditions were reported by Morishita et al. (2005) and are summarized in Table S3. Zircons mounts were etched in a NaOH–KOH eutectic melt at 220 ± 5 °C (Garver, 2003) for 60 - 90 min. Apatite mounts were etched in 5.5N HNO3 at 20±1 ºC for 20 seconds to reveal spontaneous tracks (e.g., Gleadow et al., 1984).

The intensity of the Uranium signal was calibrated against silicate glass reference material SRM 610 produced by the National Institute of Standards and Technology (NIST 610) (Longerich et al, 1996) in which the 238U concentration is 456 ppm (Carpenter and Reimer, 1974; Pearce et al., 1997). 43Ca was used as an internal standard for apatites, using chemical data obtained previously (e.g., Barbarand et al., 2003). While, 29Si as an internal standard and tacking the chemical composition from (Longerich et al., 1996; Pearce et al., 1997).

NIST SRM 612 was used as a secondary standard for the U-concentration measurements, yielded a concentration of (37.7 ± 0.7 μg/g) with concordance to the published reference values (Carpenter and Reimer, 1974; Walder et al., 1993; Pearce et al., 1997). Ages and error ranges were calculated using the methods of Vermeesch (2017) which are implemented in IsoplotR (Vermeesch, 2018).

S3.2 Thermal History Modelling

During this study, all the AFT data (single grain cooling ages, c-axes projected HCTs, Dpar) were modeled using the multi-kinetic annealing model of Ketcham et al. (2007). Initial Neoproterozoic aged (at depth), near-surface before the Cambrian (as the ANS was eroded by this time), ZFT ages (whenever dated), AFT ages, and the Suez rift opening age were used as t–T constraints (see Supplementary Material Table S1). The thermal history during the Neoproterozoic is not constraint by the fission track length data, the well-documented Neoproterozoic formation age and the Precambrian entire erosion of the ANS high topography document for huge amount of rock exhumation at the time between rock crystallization and the Cambrian. To approach the most likely cooling history (best fit t–T path), the initial inverse modeling was based on the best forward model with excellent fit to the inputted thermochronologic data, and wide t-T constrain boxes (initial cooling, the Cambrian surfaced, ZFT age, AFT age, and the Gulf of Suez initiation) were used to test the behavior of the t-T paths with a high degree of freedom. The models principally were run with 200,000 t–T paths tried (iteration). In HeFTy, each modeled t-T path has a goodness of fit (GOF) value which refers toǫ-value for comparison between the model predic-

tion and the input data. Paths with GOF values <0.05 are rejected (do not appear as possible t-T paths), ≥0.05 (≥5%) are labeled as acceptable paths (displayed in green), and GOF values ≥0.5 (≥50%) as good paths (displayed in purple). The program also displays the best GOF path in black and the weighted mean path in blue of the GOF value (Ketcham 2009; Ketcham et al. 2009).

Supplementary Figures

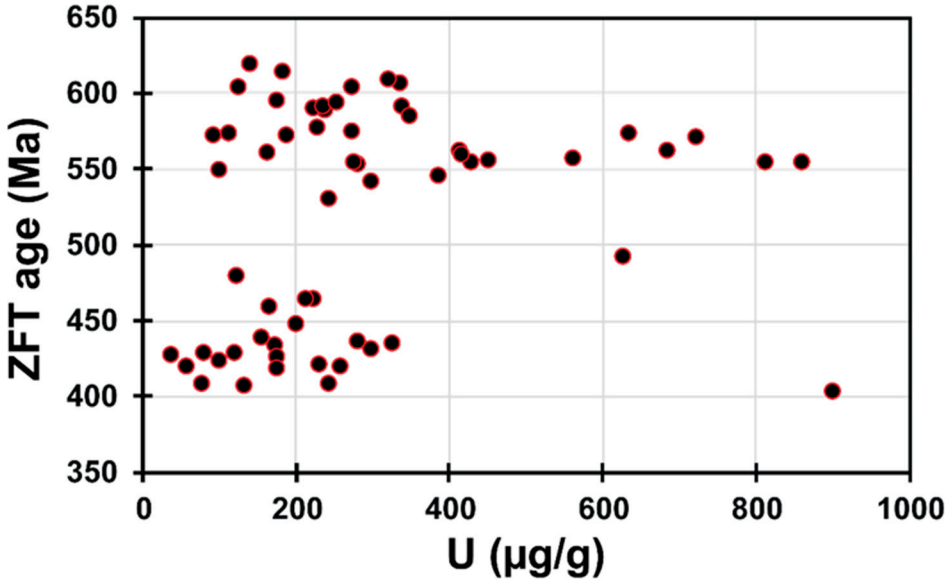

Figure S1. A plot of ZFT age versus uranium concentration does not show any systematic trend, thus ruling out a major effect of Metamictization on the ZFT data.

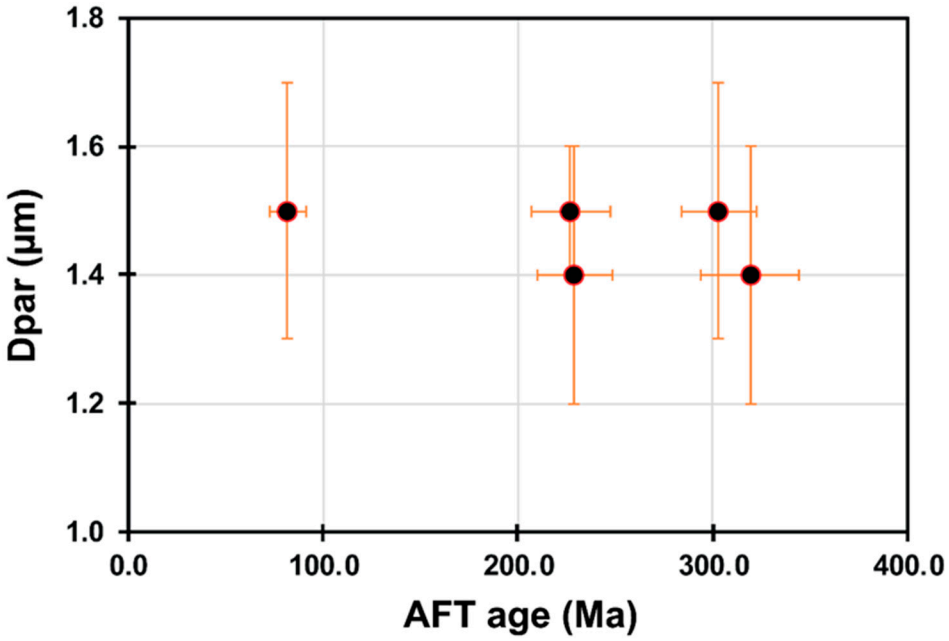

Figure S2. Dpar-AFT age plot. AFT ages show no significant change with a change in Dpar values indicating the absence of apatites chemistry differentiation on the corresponding AFT ages.

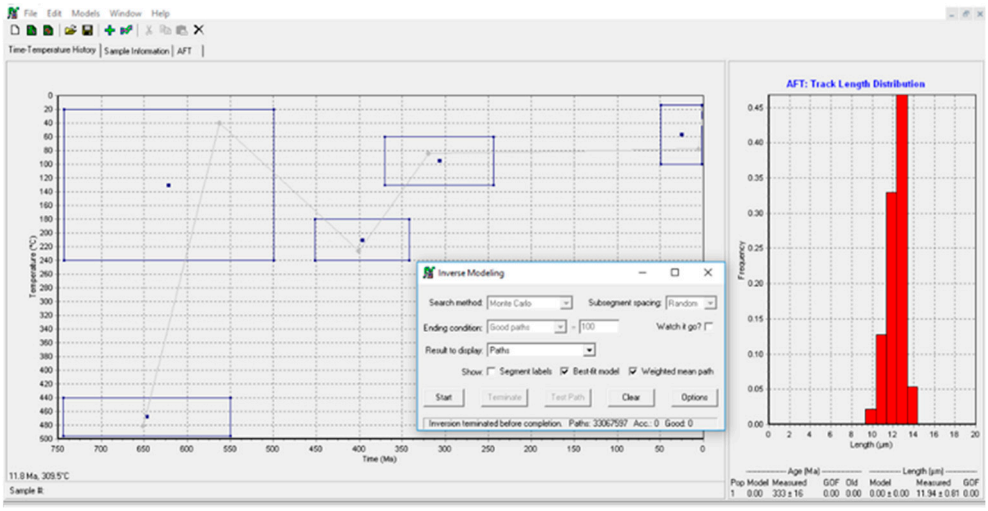

Figure S3. Thermal history modeling was obtained using HeFTy (Ketcham et al., 2009). This figure show sample SA-13 which belongs to the older ZFT age group, when tested with the same constraints (as shown here) as other samples, it shows no possible t-T scenarios even after 200 thousand iterations.

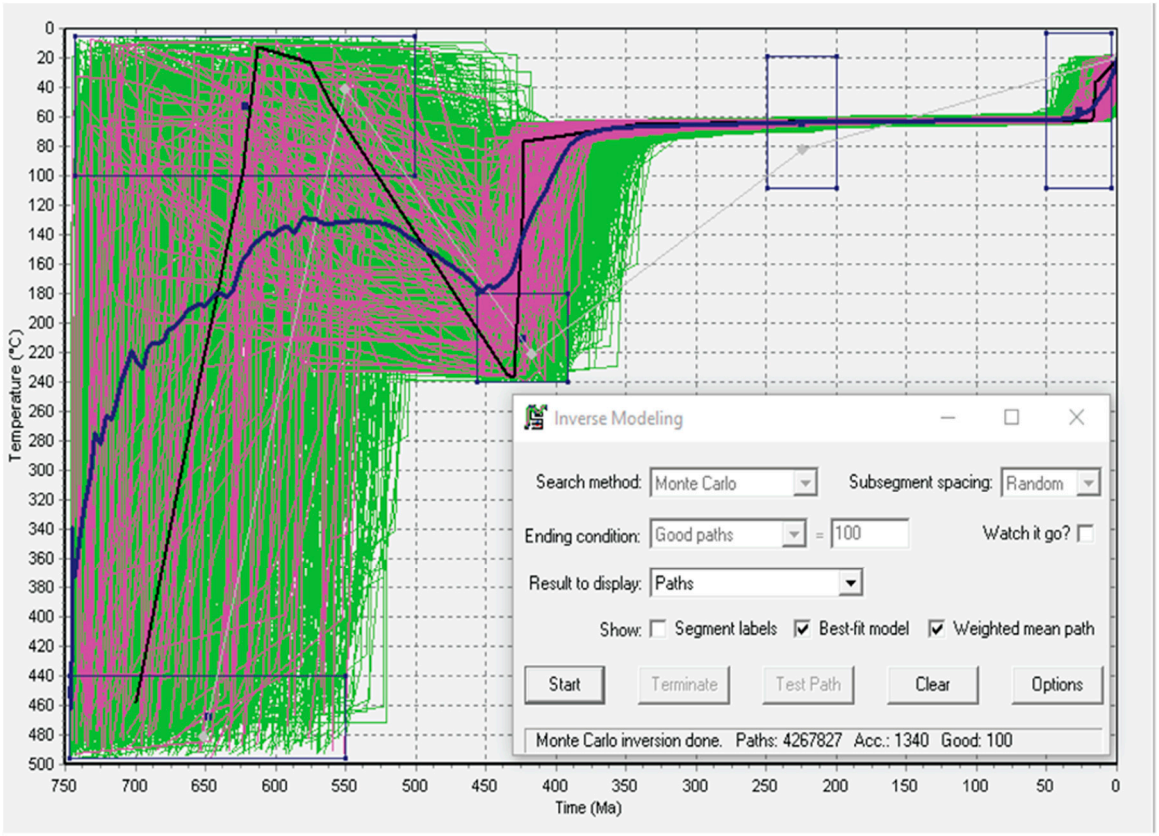

Figure S4. Thermal history modeling was obtained using HeFTy (Ketcham et al., 2009). This figure shows our examination of the possibility of having higher temperatures during the AFT constraint as the provided t-T paths were restricted to their top part at ca. 60℃.

Supplementary Tables

Table S1. The specifications of the time-temperature modeling used constraints.

Sample No.	Elev. (m.a.s.l)	Const. No.	Const. Type	T-T segment (°C)	t-t Segment (Ma)	Comments
Figure 4						

SA-13	789	1	Initial	500-440	750-375	Wider time to check the possibility of late cooling
		2	PAEE	240-20	750-372	t-T paths show subsurface possibilities
		3	AFT	110-60	350-250	mixed age, t-T migrate cooler to ca. 60 ˚C
		4	Rifting	100-20	50-0	
SA-03	624	1	Initial	500-440	750-550	
		2	PAEE	100-20	750-500	t-T paths show both surfaces and buried possibilities
		3	ZFT	240-180	450-400	
		4	AFT	110-60	200-250	mixed age, t-T migrate cooler to ca. 60 ˚C
		5	Rifting	100-20	50-0	
SN-01	371	1	Initial	500-440	750-550	
		2	PAEE	100-20	750-500	t-T paths show both surfaces and buried possibilities
		3	ZFT	240-180	500-400	
		4	AFT	110-60	100-50	mixed age, t-T migrate cooler to ca. 60 ˚C
		5	Rifting	100-20	50-0	
SA-01	458	1	Initial	500-440	750-550	
		2	PAEE	100-20	750-500	t-T paths show both surfaces and buried possibilities
		3	ZFT	240-180	550-300	Wide time constraint as no ZFT age dated
		4	AFT	110-60	100-50	mixed age, t-T migrate cooler to ca. 60 ˚C
		5	Rifting	100-20	50-0	

The time and temperature used specifics for each constraint that guide the t-T paths of the thermal history modeling. Specifics for each constraint were standardized, however, changes in time and temperature limits were made for constraints from sample to sample based on the degree of uncertainty, to give a higher degree of freedom or to test other scenarios.

Table S2. Operating conditions for the LA-ICP-MS.

Table S2. Operating conditions for the LA-ICP-MS.	
ICP-MS	
Model	Agilent 7500s
Forward power	1200 W
Reflected power	1 W
Carrier gas flow	1. 31/min^{-1} (Ar)
	0.31/min^{-1} (He)
Auxiliary gas flow	1.01/min^{-1}
Plasma gas flow	151/min^{-1}
Interface	Ni sample cone
	Ni skimmer cone
Laser	
Model	MicroLas GeoLas Q plus
Wavelength	193 nm (Excimer ArF)
Repetition rate	5 Hz
Pulse energy	8 J/cm^2
Pit diameter	20 μm